Numerical analysis and optimization of surface textures for a tilting pad thrust bearing

Daniel Gropper, Terry J. Harvey, Ling Wang

PII: S0301-679X(18)30179-8

DOI: 10.1016/j.triboint.2018.03.034

Reference: JTRI 5178

To appear in: *Tribology International*

Received Date: 6 February 2018

Revised Date: 27 March 2018

Accepted Date: 30 March 2018

Please cite this article as: Gropper D, Harvey TJ, Wang L, Numerical analysis and optimization of surface textures for a tilting pad thrust bearing, *Tribology International* (2018), doi: 10.1016/j.triboint.2018.03.034.

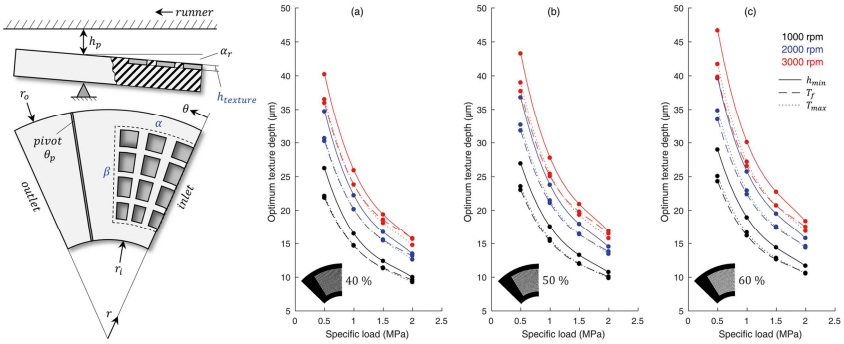

Numerical analysis and optimization of surface textures for a tilting pad thrust bearing

Daniel Gropper *, Terry J. Harvey, Ling Wang

[1] *National Centre for Advanced Tribology at Southampton (nCATS), Faculty of Engineering and the Environment, University of Southampton, Southampton SO17 1BJ, UK*

*Corresponding author. E-mail address: D.Gropper@soton.ac.uk

Abstract

A thermo-hydrodynamic model previously developed by the authors is applied in this paper to study the influence of surface texturing on the performance of a tilting pad thrust bearing with offset line pivots. Utilizing an interior-point algorithm, texture depth, circumferential extent and radial extent are numerically optimized to improve three bearing performance parameters: minimum film thickness, friction torque and maximum temperature. Results are presented for various operating conditions and texture densities. It is found that, for most cases, optimum texturing parameters depend significantly on the operating conditions, optimization objective and texture density. Whereas minimum film thickness values can be increased by up to 12 %, only minor improvements are achievable in terms of friction torque and maximum temperature.

Keywords: Surface texturing, Tilting pad thrust bearings, Numerical analysis

Nomenclature

a	coefficient for viscosity temperature relationship
c_p	lubricant specific heat (J/kg/K)
e_p, e_e, e_t	tolerance value for pressure, equilibrium and temperature solver
e_o	optimality tolerance
h	local film thickness (m)
h_p	film thickness at pivot (m)
$h_{texture}$	texture depth (m)
k	iteration
k_{con}	convection parameter
l	texture arc length at mid radius
m, n	coefficients for viscosity temperature relationship
p	local pressure (Pa)
Q	volumetric flow rate (m^3/s)
Re	Reynolds number
S	relative texture depth
r	radial coordinate (m)
r_i	inner pad radius (m)
r_o	outer pad radius (m)
T	temperature (°C)
T_f	friction torque (Nm)
$T_{\circ K}$	temperature (°K)
U	runner velocity (m/s)
W_0	applied load (N)
$\boldsymbol{x}$	texture design vector
α	relative texture extent in circumferential direction
α_r	pitch angle (rad)
β	relative texture extent in radial direction
δW	difference in load carrying capacity and applied load (N)
$\delta\theta$	circumferential distance from centre of pressure to pivot (rad)
$\varepsilon_p, \varepsilon_e, \varepsilon_t$	fractional residuals for pressure, equilibrium and temperature

	solver
ε_o	first order optimality
η	lubricant dynamic viscosity (Pa.s)
Θ	fractional film content
θ	circumferential coordinate (rad)
θ_p	circumferential coordinate of pivot (rad)
λ	texture aspect ratio
ν_{cSt}	lubricant kinematic viscosity (cSt)
Π	frictional power loss (W)
ρ	lubricant density (kg/m^3)
$\rho_{texture}$	texture density
ω	rotational speed (1/s)

1 Introduction

Although first papers on the application of artificial surface textures for enhancing the performance of tribological contacts were published decades ago, a large quantity of research is still being conducted. This is mainly due to the lack of universal texture design recommendations, as it has become clear that, despite the fact that surface textures can be optimized, the optimum design depends significantly on the application, the lubrication regime and even the operating conditions [1]. One of the most popular applications of surface texturing are hydrodynamic bearings, where the main aim is a performance improvement in terms of minimum film thickness, friction torque, temperature and wear.

This paper is concerned with textured tilting pad thrust bearings, an application of surface texturing that has hardly been given any attention. One of the only studies was published recently by Zouzoulas and Papadopoulos [2]. They compared the hydrodynamic performance of a conventional **point-pivoted** tilting pad thrust bearing with a pocketed, grooved and dimpled design using commercial CFD software. The results showed that minimum film thickness, friction torque and maximum temperature can be improved considerably. Best performance improvements were achieved by the pocketed bearing, followed by the one having circumferential grooves. A parametric study revealed the dependency of optimum texturing parameters on the operating condition and optimization objective. For the investigated cases, a texture depth of 30 µm and a radial texture extent of around 70 % were recommended.

Considerably more studies are available concerning fixed geometry thrust pad bearings. Marian et al. [3], for example, presented a parametric numerical study on a parallel thrust pad bearing with square dimples and recommended circumferential and radial texture extents of 50 % and from 90 to 100 % respectively in terms of load carrying capacity. Henry et al. conducted experiments on textured parallel thrust bearings under static hydrodynamic conditions [4] as well as start-up conditions [5]. Under static hydrodynamic conditions, it was found that texturing can significantly improve bearing performance in terms of friction torque and minimum film thickness. Under start-up conditions, texturing was able to decrease the peak in friction torque although some of the investigated texture designs prolonged the time required to establish purely hydrodynamic lubrication. Fouflias et al. [6] compared the performance of textured, pocketed and tapered-land parallel thrust pad bearings via CFD and concluded that the pocketed pads result in highest load carrying capacities. In a later study

[7], they numerically optimized pocket dimensions and shape utilizing Genetic algorithms. Another optimization study was published by Papadopoulos et al. [8] for convergent thrust pad bearings. They showed that the optimum texture extent in circumferential direction and the optimum texture depth depend on the convergence ratio and that the highest possible texture density should be chosen. Papadopoulos et al. [9] presented a parametric CFD study and concluded that 67 % and 75 % of the pad should be textured in circumferential and radial direction respectively in terms of load carrying capacity. Moreover, a texture depth close to the encountered minimum film thickness was recommended.

Although these findings are to a certain extent applicable to pivoted pad bearings, more research is needed for this application; in particular regarding the influence of surface texturing on the equilibrium position of the pads. Moreover, previous research is generally limited to only a few operating conditions and restricted parametric studies due to the complexity of the flow and associated high computation times. No optimization of surface patterns has been performed previously for tilting pad bearings.

The present paper is focussed on optimizing texture patterns for tilting pad thrust bearings and investigate their dependency on the optimization objective and operating condition. To allow a mathematical optimization for various conditions in reasonable time, a fast numerical model previously developed by the authors finds application [10]. The model utilizes an adaptive and non-uniform finite volume discretization, where discontinuities are directly incorporated in the discrete system. Moreover, the computational speed is improved by taking advantage of multicore processing, using results from the equivalent untextured bearing and evaluating the bearing equilibrium through a combination of the Newton-Raphson method and Broyden's algorithm. In this paper, the previously developed model is applied in combination with an interior-point method to mathematically optimize texture designs in terms of circumferential extent, radial extent and texture depth for three optimization objectives: a maximization of the encountered minimum film thickness, a minimization of frictional torque and a minimization of the maximum temperature. An in-depth analysis regarding the dependency of the optimum texture design on the operating conditions and optimization objective as well as achievable performance improvements under hydrodynamic conditions are presented. Furthermore, texture design recommendations are given for a wide range of conditions.

2 Model setup

The thermo-hydrodynamic model applied in this paper is described in detail in Ref. [10] and is therefore only given briefly in the following.

2.1 Bearing and texture geometry

The bearing considered is a partially textured tilting pad thrust bearing with offset line pivots (see Fig. 1).

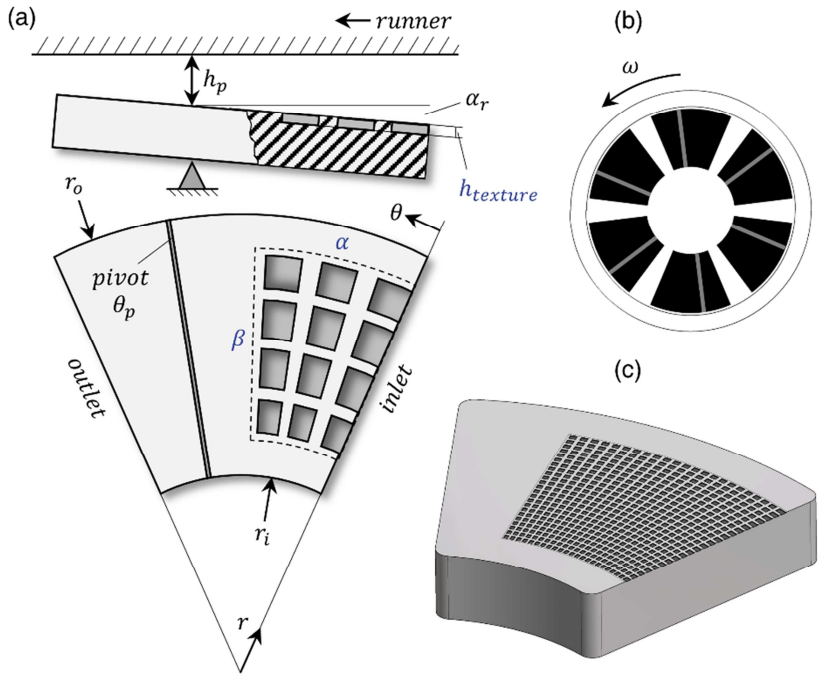

Fig. 1 (a) Pad details with coordinate system, (b) tilting pad thrust bearing geometry and (c) exemplary texture pattern with $\alpha = 70$ %, $\beta = 70$ %, $h_{texture} = 10$ µm *and* $\rho_{texture} = 40$ %.

Only partial texturing is considered as it is well known from literature that partial texturing outperforms full texturing for the case of parallel pad bearings [1]. The pads have an inner radius of 30.25 mm, an outer radius of 70.25 mm and span an angle of 46.05° with the pivot being located at 60 % from the inlet. Although it is known from literature that a pocketed or grooved design may provide better performance for parallel and convergent contacts under hydrodynamic conditions [1], the chosen surface pattern consists of 529 individual angular sector shaped textures with flat bottom profile arranged in a 23 x 23 grid. This design was chosen as individual textures may act as lubricant reservoirs and trap wear debris and therefore outperform a pocketed pad under critical mixed lubrication conditions while still providing reasonable performance under hydrodynamic conditions. The first row of textures is elongated towards the inlet to promote lubricant supply **and only angular sector shaped textures are considered to most closely approximate a pocketed**

configuration as recommended in literature [1]. The texture pattern is fully defined by four parameters: The texture depth ($h_{texture}$), the circumferential extent of the textured area (α), the radial extent of the textured area (β) and the texture density ($\rho_{texture}$). The film thickness over the pad area can be expressed as

$$h(\theta, r) = h_p + r \sin(\theta_p - \theta) \sin \alpha_r \tag{1}$$

where h_p is the film at the level of the pivot, θ_p the angular location of the pivot and α_r the pitch angle. The texture depth is simply added wherever textures are located during the numerical preparation of the film **thickness** distribution.

2.2 Fluid mechanics

The incompressible Reynolds equation is applied to evaluate the pressure distribution over the pad area. In polar coordinates and incorporating mass-conserving cavitation, the applied Reynolds equation reads

$$\frac{\partial}{\partial r}\left(r\frac{\rho h^3}{\eta}\frac{\partial p}{\partial r}\right) + \frac{1}{r}\frac{\partial}{\partial \theta}\left(\frac{\rho h^3}{\eta}\frac{\partial p}{\partial \theta}\right) = 6\omega r \frac{\partial(\Theta \rho h)}{\partial \theta} \tag{2}$$

where p is the local pressure, ρ the lubricant density, ω the rotational speed, η the dynamic viscosity and Θ the fractional film content as described in [11, 12] **to incorporate JFO boundary conditions**. A modified adaptive non-uniform finite volume method is applied to discretize the equations, where discontinuities are directly incorporated in the discrete system to reduce discretization errors and computation time [13]. Although the approach allows the consideration of concentrated inertia effects, they are disregarded in the present study for improved computational performance. This is justified by the low Reynolds numbers and high texture aspect ratios encountered. Dobrica and Fillon [14] showed that the validity of the Reynolds equation for textured surfaces depends on these two parameters. Here, the Reynolds number is defined as $Re = \rho U h_{min}/\eta$ and the texture aspect ratio as $\lambda = l/h_{texture}$, where l is the arc length at the mid radius of the texture. Re varies over the pad area due to local changes in viscosity (caused by the local changes in temperature) and runner velocity. λ varies with the radius, as the textures are defined using a constant angular span. Hence, multiple combinations of Reynolds numbers and aspect ratios are encountered for each simulation. For all performed simulations, Re ranges from 1 to 36 and λ from 8 to 104. Encountered combinations result in good agreement between the Reynolds and Navier-Stokes models with respect to the predicted load carrying capacity.

The mesh is adapted to the investigated texture pattern by aligning control volume boundaries with discontinuities. The mesh is defined by the number of control volumes inside individual textures, in-between adjacent textures as well as the number of control volumes for the untextured portions of the pad (see Fig. 2).

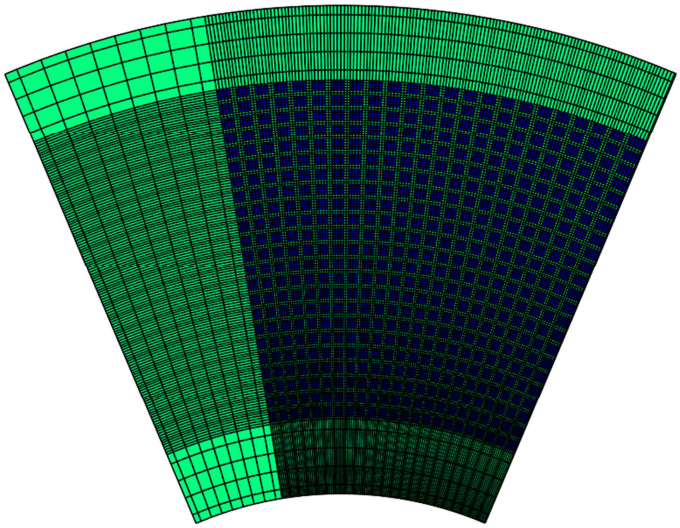

Fig. 2 Computational mesh with 4 x 4 control volumes inside individual textures, 2 x 2 control volumes in-between adjacent textures, 8 control volumes for the untextured pad area in circumferential direction and 4 control volumes each for the untextured pad areas in radial direction.

The utilized mass-conserving cavitation algorithm requires an iterative solution of the discrete Reynolds equation [12], therefore, a Gauss-Seidel method with pointwise relaxation is applied for both pressure and film content. A constant pressure at the pad boundaries (10^{-5} Pa) and no-slip conditions are imposed. The iteration stops when the fractional residual reaches values smaller than or equal to a pre-defined tolerance value (for this work $e_p = 10^{-6}$).

$$\varepsilon_p = \sum_{j=2}^{jj-1}\sum_{i=2}^{ii-1}\frac{\left|p_{i,j}^{k} - p_{i,j}^{k-1}\right|}{\left|p_{i,j}^{k}\right|} + \sum_{j=2}^{jj-1}\sum_{i=2}^{ii-1}\frac{\left|\Theta_{i,j}^{k} - \Theta_{i,j}^{k-1}\right|}{\left|\Theta_{i,j}^{k}\right|} \leq e_p \tag{3}$$

2.3 Bearing equilibrium

The bearing equilibrium is found by a combination of the Newton-Raphson method and Broyden's method with Sherman-Morrison formula, where the Jacobian matrix is evaluated using a perturbation approach and finite difference formulae. The Newton-Raphson method is applied only for the first temperature iteration. The equilibrium for following temperature iterations is evaluated with Broyden's method for enhanced computational speed due to the

time saved in the determination of the Jacobian matrix. **For details about the applied methods and formulae the reader is referred to Ref. [10]**. The convergence of the equilibrium solver is checked by the following criterion:

$$\varepsilon_e = \frac{|\delta W|}{W_0} + \frac{|\delta \theta|}{\theta_p} \leq e_e \tag{4}$$

where a tolerance value of $e_e = 10^{-4}$ is used.

2.4 Thermal effects

The lubricant temperature is evaluated using an effective temperature method, where a convection parameter of $k_{con} = 0.75$ is used [15, 16], i.e. it is assumed that 75 % of the heat caused by viscous shearing is removed by convection:

$$T_{eff} = T_{inlet} + k_{con} \frac{\Pi}{Q_{in} \rho c_p} \tag{5}$$

T_{inlet} is the temperature at the pad inlet, Π the frictional power loss, Q_{in} the lubricant inflow and c_p the specific heat of the lubricant. The inlet temperature rise due to the hot-oil-carry-over effect is considered according to Refs. [2, 17]. The maximum temperature is approximated empirically by $T_{max} = 2T_{eff} - T_{inlet}$ and McCoull and Walther's equation is applied to calculate the temperature dependent viscosity [16]:

$$log_{10}[log_{10}(\nu_{cSt} + a)] = n - m log_{10}(T_{°K}) \tag{6}$$

The bearing is supplied with ISO VG 32 oil ($a = 0.6$, $n = 9.6487$, $m = 3.7940$, $\rho = 875$ kg/m^3, c_p =2035 J/kg/K) at a constant temperature of 30 °C and a flow rate of 1.85 l/min per pad. Temperatures and viscosity are computed iteratively. The procedure stops when temperature convergence is reached according to

$$\varepsilon_t = \frac{\left|T_{eff}^{k+1} - T_{eff}^{k}\right|}{T_{eff}^{k+1}} \leq e_t \tag{7}$$

where the tolerance value used in this work is $e_t = 10^{-5}$.

2.5 Texture optimization

The optimization of a given texture design involves finding the texturing parameters that minimize or maximize a certain bearing performance parameter. In the present study, three optimization objectives are investigated: (i) the maximization of the minimum film thickness

(ii) the minimization of the friction torque and (iii) the minimization of the maximum temperature. These can be expressed as nonlinear constrained optimization problems:

$$\max_x h_{min}(\boldsymbol{x}) \text{, subject to } \boldsymbol{x}_{min} \leq \boldsymbol{x} \leq \boldsymbol{x}_{max} \quad (8)$$

$$\min_x T_f(\boldsymbol{x}) \text{, subject to } \boldsymbol{x}_{min} \leq \boldsymbol{x} \leq \boldsymbol{x}_{max} \quad (9)$$

$$\min_x T_{max}(\boldsymbol{x}) \text{, subject to } \boldsymbol{x}_{min} \leq \boldsymbol{x} \leq \boldsymbol{x}_{max} \quad (10)$$

where $\boldsymbol{x}$ is a vector containing the texture design parameters $\boldsymbol{x} = (h_{texture}, \alpha, \beta)^t$. $\boldsymbol{x}_{min}$ and $\boldsymbol{x}_{max}$ are the lower and upper bound constraints for this vector, here $\boldsymbol{x}_{min} = (0\ \mu\text{m}, 10\ \%, 10\ \%)^t$ and $\boldsymbol{x}_{max} = (75\ \mu\text{m}, 95\ \%, 95\ \%)^t$. The texture density cannot be optimized, as the optimum density is always 100 % [1]. Therefore, three fixed densities are investigated here: 40 %, 50 % and 60 %. The optimization is performed in MATLAB with the function *fmincon* [18] utilizing an interior-point algorithm and forward finite difference estimates. Multiple processor cores are utilized to evaluate the gradients of the objective functions and start values of $\boldsymbol{x} = (10\ \mu\text{m}, 50\ \%, 50\ \%)^t$ and a step tolerance of 10^{-8} are used. The procedure stops when the first order optimality is equal to or below the optimality tolerance: $\varepsilon_o \leq e_o = 10^{-5}$.

2.6 Numerical procedure

After importing the input file, the numerical procedure starts by preparing the mesh and initializing the film thickness distribution (see Fig. 3).

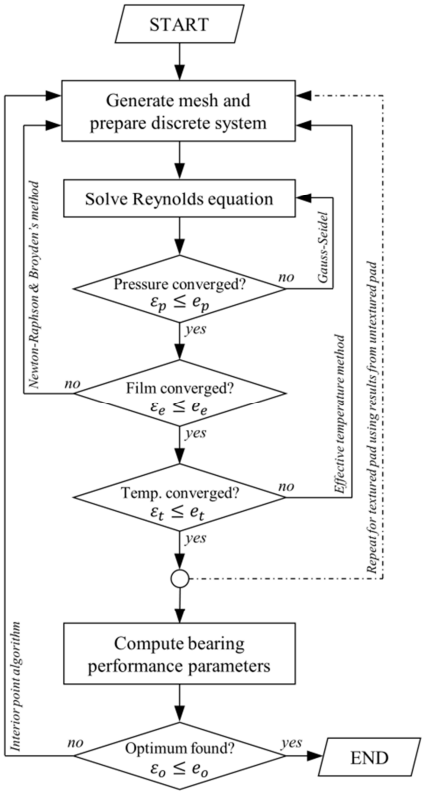

Fig. 3 Simplified flow chart for the numerical texture design optimization.

After this, the discrete Reynolds equation is assembled and solved using the Gauss-Seidel method until pressure convergence is reached ($\varepsilon_p \leq e_p$). The film thickness distribution is then updated by the Newton-Raphson and Broyden's method until the pad is in equilibrium ($\varepsilon_e \leq e_e$). The effective temperature method is subsequently applied to update inlet temperature, effective temperature and effective lubricant viscosity until thermal equilibrium is reached ($\varepsilon_t \leq e_t$). This series of steps is initially executed for the equivalent untextured pad, where a coarse uniform mesh is used, and then repeated for the textured pad using all results from the untextured pad. This methodology leads to a significant reduction in computation time [10]. What follows is the computation of the objective functions as well as other important bearing performance parameters, such as tilt angle, power loss and flow rates. To evaluate the gradients of the objective functions, the above computations are performed simultaneously on the available processor cores for different texture design vectors $\boldsymbol{x}$. The interior-point algorithm then updates the texture design to minimize or maximize the objective function until the optimality tolerance reaches the specified tolerance ($\varepsilon_o \leq e_o$).

3 Computational results

The numerical model was developed with MATLAB 2016b and all simulations are performed on a desktop workstation with *Intel Core i7-3770* @ 3.40 GHz CPU and 16 GB of RAM.

3.1 Mesh study

To ensure accurate results, a number of mesh studies are conducted for a reference case, where the bearing runs at 1000 rpm and a film thickness similar to the one encountered at an operation at a specific load of 1.0 MPa. A texture design with $\alpha = 70\%$, $\beta = 70\%$ and $h_{texture} = 15$ µm is considered for this purpose. The mesh studies are based on the predicted load carrying capacity as this was found to be the parameter most influenced by the mesh size based on numerous test simulations. Computations are performed for 10 meshes, ranging from 5476 to 288369 degrees of freedom for texture densities of 40%, 50% and 60%. The results are plotted in Fig. 4 in terms of the difference in predicted load carrying capacity with respect to the load carrying capacity computed with the finest mesh.

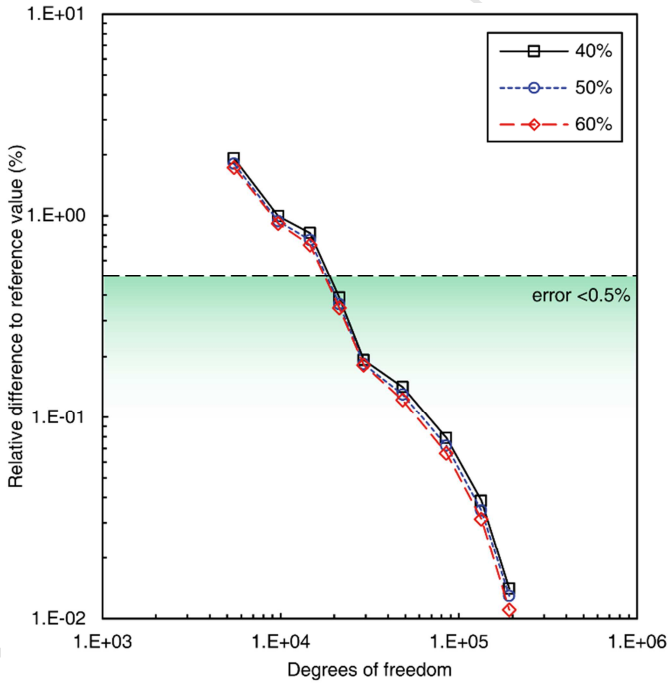

Fig. 4 Results of the mesh study for texture densities of 40%, 50% and 60%.

It can be seen that, independent of the texture density, the mesh with 21316 degrees of freedom results in a deviation of less than 0.5%. Therefore, all simulations presented in this paper are conducted with this mesh, consisting of 4 control volumes inside each individual texture, 2 control volumes in-between adjacent textures, 8 textures for the untextured pad

area in circumferential direction and 4 control volumes each for the untextured pad areas in radial direction (this mesh is shown in Fig. 2).

3.2 Validation

The accuracy of the applied numerical model in terms of h_{min}, T_f and T_{max} was investigated in detail in Ref. [10] by comparison with CFD results. It was shown that average deviations to CFD were 5.3, 1.4 and 3.6 % with respect to minimum film thickness, friction toque and maximum temperature respectively. Therefore, only the numerical implementation and convergence of the optimization procedure based on the interior-point algorithm is analysed here. For this purpose, an exhaustive parametric study is performed for a thrust pad with $\rho_{texture} = 50\,\%$ operating at 1000 rpm and 1.0 MPa specific load. The objective functions are evaluated for a total of 1573 texture designs parameterized as follows: $30\,\% \leq \alpha \leq 80\,\%$ (step 5 %), $30\,\% \leq \beta \leq 90\,\%$ (step 5 %) and $5\,\mu m \leq h_{texture} \leq 30\,\mu m$ (step 2.5 µm). The optimization is then performed for four different start values at the corners of the parameter space: $\boldsymbol{x}_{start,1} = (10\,\mu m, 30\,\%, 30\,\%)^t$, $\boldsymbol{x}_{start,2} = (10\,\mu m, 80\,\%, 90\,\%)^t$, $\boldsymbol{x}_{start,3} = (30\,\mu m, 30\,\%, 90\,\%)^t$, $\boldsymbol{x}_{start,4} = (30\,\mu m, 80\,\%, 30\,\%)^t$.

Fig. 5 shows the parametric results in terms of the relative difference to the optimum value as well as the paths of the optimization algorithm, where iterations of the interior-point algorithm are indicated by black “x” markers and start and end values by black and yellow circles respectively.

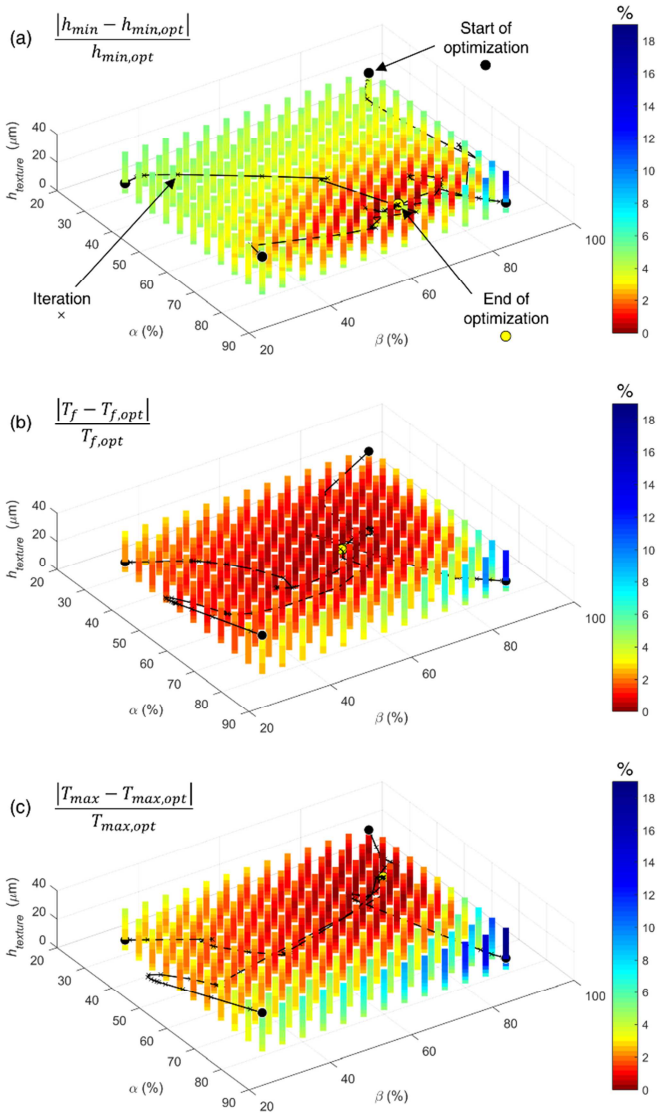

Fig. 5 Validation of the optimization algorithm for the three optimization objectives: (a) minimum film thickness, (b) friction torque and (c) maximum temperature.

Based on the optimality tolerance, the interior-point algorithm converges for all cases, needing between 26 and 43 iterations. Furthermore, the prediction of the optimum texturing parameters is independent of the start value. Within the parameter space investigated, local minima (maxima) are also global minima (maxima), indicating a successful optimization.

It is noticeable that the optimum texture design does, however, depend on the optimization objective. Whereas the optimum texture depth is fairly independent of the optimization objective (15.2 µm $\leq h_{texture,opt} \leq$ 17.5 µm), the optimum extents of the textured area show a significant dependence on the optimization objective; for the presented case: 41 % $\leq \alpha_{opt} \leq$ 72 % and 68 % $\leq \beta_{opt} \leq$ 86 %. It is further observable that the area around the optimum texture design where the objective function value is only a few percent away from

its optimum is different for the three optimization objectives. Whereas the minimum film thickness is very sensitive to a change in texturing parameters around the optimum, reasonably good friction and temperature characteristics can be achieved with a texture design that is a bit further away from the optimum. This means that, for the considered cases, the chosen texture design would most likely be based on the design resulting in the highest minimum film thickness.

3.3 Optimization results

The texture design optimization is performed for a total of twelve operating conditions (1000, 2000, 3000 rpm at 0.5, 1.0, 1.5, 2.0 MPa), three optimization objectives (h_{min}, T_f, T_{max}) and three texture densities (40, 50, 60 %), resulting in a total of 108 simulations. The required computation time for each optimization was around 40 minutes. Note that a cubic spline interpolation is used to smoothen the graphs presented in the following.

3.3.1 Optimum texture depth

Results of the optimization in terms of the optimum texture depth are shown in Fig. 6.

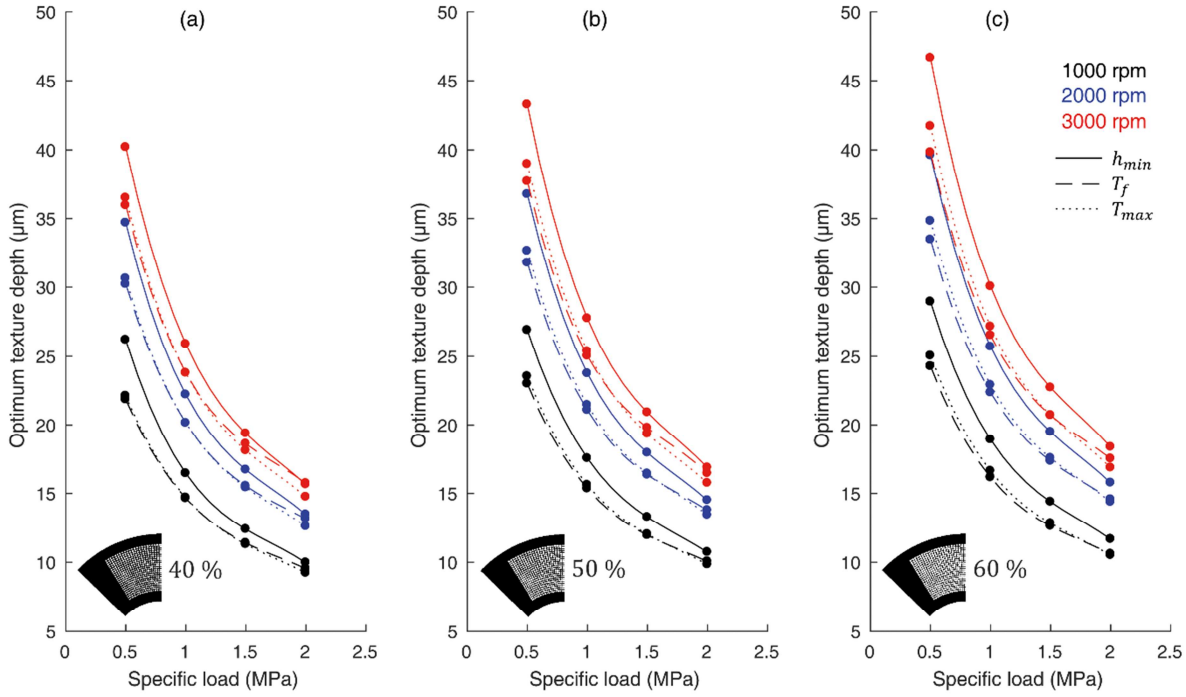

Fig. 6 Optimum texture depth for different operating conditions and optimization objectives for a texture density of (a) 40 %, (b) 50 % and (c) 60 %.

The results show that the optimum texture depth depends on the applied load and speed, the optimization objective as well as the texture density, ranging from 9 to 47 µm. A clear

relation between the optimum texture depth and the operating condition is present for all **12** cases considered, where $h_{texture,opt}$ increases with an increase in speed and decreases with an increase in load, indicating a dependency of $h_{texture,opt}$ on the minimum film thickness. The results further demonstrate that the optimum texture depth depends on the texture density, where a higher density entails deeper textures. The optimization objective does have an impact on the optimum texture depth as well. Whereas predicted values for $h_{texture,opt}$ are almost identical for the optimization of T_f and T_{max}, values are considerably higher when the bearing is optimized in terms of h_{min} (on average about 11 %).

To further analyse the relation between the optimum texture depth and the minimum film thickness, results are plotted again in terms of the relative texture depth defined as $S = h_{texture}/h_{min}$, where h_{min} is taken from the equivalent untextured bearing rather than the texture bearing to allow a selection of the texture depth based on easily available data from the conventional bearing (see Fig. 7).

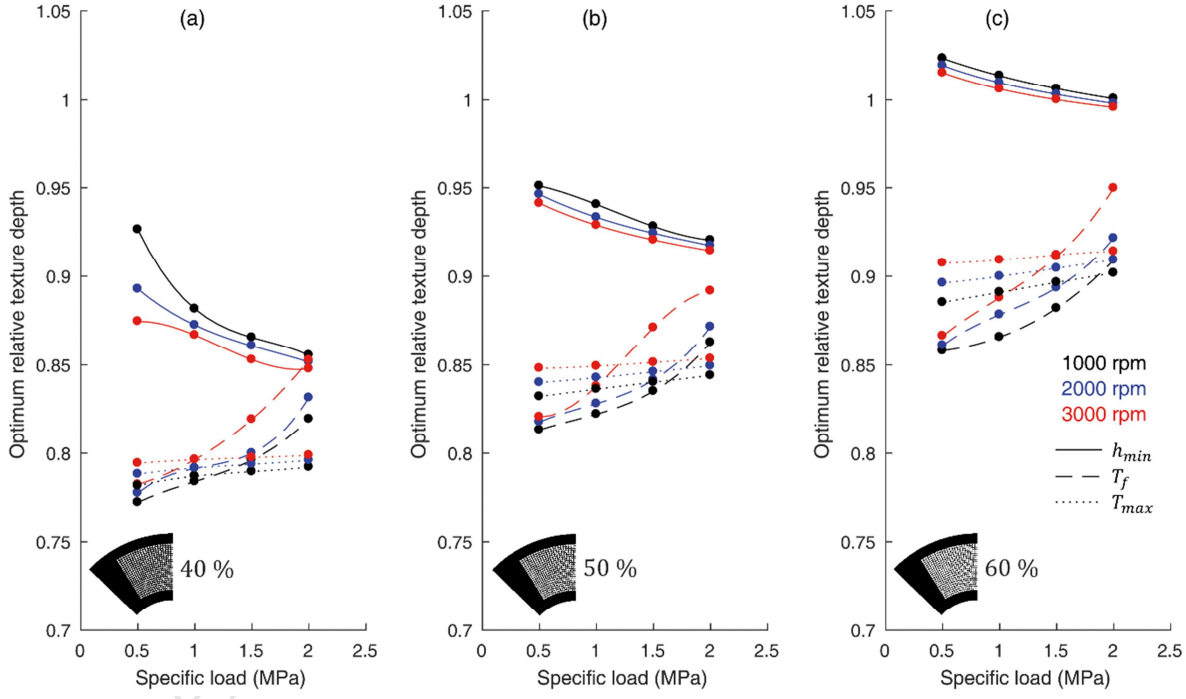

Fig. 7 Relative optimum texture depth for different operating conditions and optimization objectives for a texture density of (a) 40 %, (b) 50 % and (c) 60 %.

The optimum relative texture depth is almost independent of the rotational speed and only varies slightly with a change in applied specific load, where the optimum relative texture depth decreases with an increase in load when the pattern is optimized for h_{min} and increases with an increase in load for the other objectives. However, as the

changes are marginal and a texture depth deviating only slightly from the optimum will still result in *almost optimal* performance as presented in Fig. 5, justify the simplification of the data by averaging over the 12 investigated operating conditions. This results in a recommended relative texture depth of 0.87, 0.93 and 1.01 for densities of 40, 50 and 60 % respectively if a high minimum film thickness is desired. To optimize the bearing in terms of friction and maximum temperature, the relative texture depth should be slightly lower at 0.8, 0.84 and 0.9 for the three investigated densities. **As a rule of thumb, a relative texture depth of just under 1 seems to be preferable**. In fact, it is well known that a relative texture depth of approximately 1 results in best performance for partially textured fixed geometry parallel and near-parallel hydrodynamic contacts [1]. The found values for the relative texture depth confirm that this is also true for the case of pivoted pad bearings. Furthermore, slightly deeper textures seem be the better for increasing the minimum film thickness whereas lower texture depths are preferred for a reduction of friction and temperature. This was also concluded in the parametric CFD study for point-pivoted pads by Zouzoulas and Papadopoulos [2]. The high dependency of the optimum texture depth on bearing speed and specific load makes it clear that the texture depth has to be selected for the expected operating condition or will be a compromise for the expected range of conditions.

3.3.2 Optimum circumferential texture extent

Results for the optimum extent of the textured region in circumferential direction are given in Fig. 8.

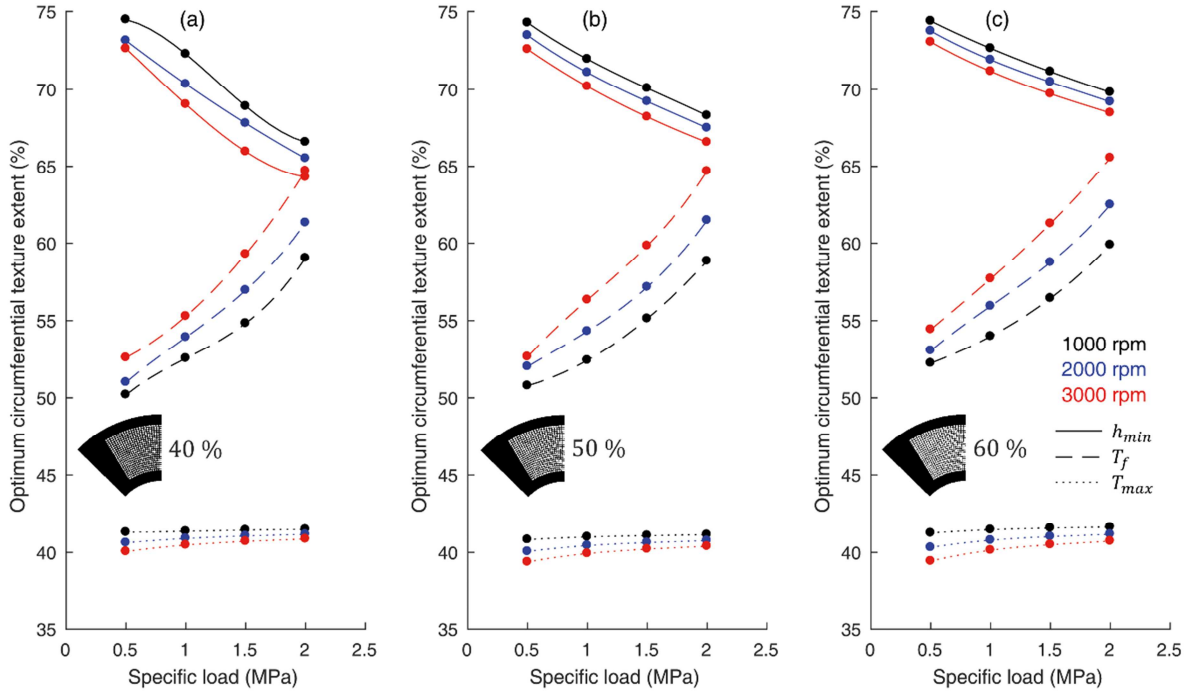

Fig. 8 Optimum circumferential texture extent for different operating conditions and optimization objectives for a texture density of (a) 40 %, (b) 50 % and (c) 60 %.

It is notable that α_{opt} is almost independent of the rotational speed as well as the texture density. However, values significantly depend on the optimization objective and specific load, ranging from 39 to 74 %. α_{opt} decreases with an increase in specific load when optimized for h_{min}, starting at about 73 % and ending at about 64 %. The opposite is the case when α is optimized for T_f, where values range from 50 % to 65%. Interestingly, α_{opt} is independent of the specific load when optimized for minimizing the maximum temperature, allowing to recommend a single value of 41 %. This can be explained by the high influence of the texture extent in circumferential direction on the centre of pressure and therefore the equilibrium of the pad in terms of the tilt angle. To minimize the maximum temperature, a high lubricant inflow is desired, which is achieved by increasing the film thickness at the pad inlet by increasing the convergence ratio or tilt angle. For the investigated bearing and pivot position, this is achieved by texturing about 41 % of the pad. The presented results show that as a rule of thumb about 3/4 of the pad should be textured in circumferential direction for maximizing the minimum film thickness, just over half of the pad for minimizing friction and about 2/5 of the pad for minimizing the maximum temperature.

3.3.3 Optimum radial texture extent

Regarding the optimum extent of the textured region in radial extent, values range from 56 to 91 % (see Fig. 9).

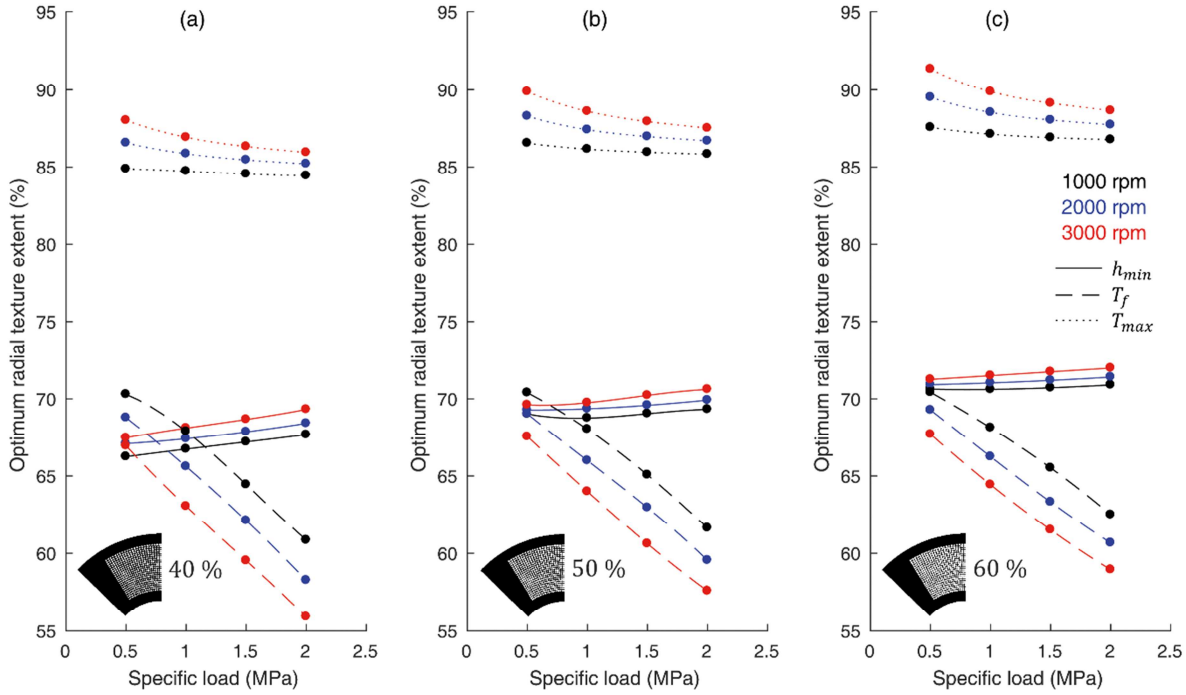

Fig. 9 Optimum radial texture extent for different operating conditions and optimization objectives for a texture density of (a) 40 %, (b) 50 % and (c) 60 %.

β_{opt} is mostly independent of the rotational speed and only shows a relevant dependency on the specific load when optimized in terms of the friction torque, where β_{opt} gets smaller with an increase in load, ranging from 70 to 56 %. It is also evident that a higher texture extent is required for higher texture densities, although differences are small. Similarly to the optimum extent in circumferential direction, the most influential parameter is the optimization objective. If optimized in terms of minimum film thickness, the radial extent should be between 66 and 72 %. Much higher values are predicted when the bearing is optimized for minimizing the maximum temperature. In this case, β_{opt} should be between 84 and 91 %. The reason behind this is that the higher the texture extent in radial direction, the higher the lubricant inflow, which promotes cooling and results in lower temperatures. In fact, the lubricant inflow is increased by 9 % on average with respect to the untextured bearing. The results show that as a rule of thumb, it can be concluded that a relatively high extent in radial direction of approximately 87 % is recommended when the objective is a minimization of the maximum temperature. About 2/3 of the pad should be textured for optimum performance regarding the minimum film thickness and good frictional behaviour.

4 Discussion

4.1 Performance of the untextured bearing

To evaluate the influence of texturing on the bearing performance, the key characteristics of the conventional untextured bearing are evaluated. For these computations, a uniform mesh with 101 x 101 control volumes is used. Results are presented in Fig. 10.

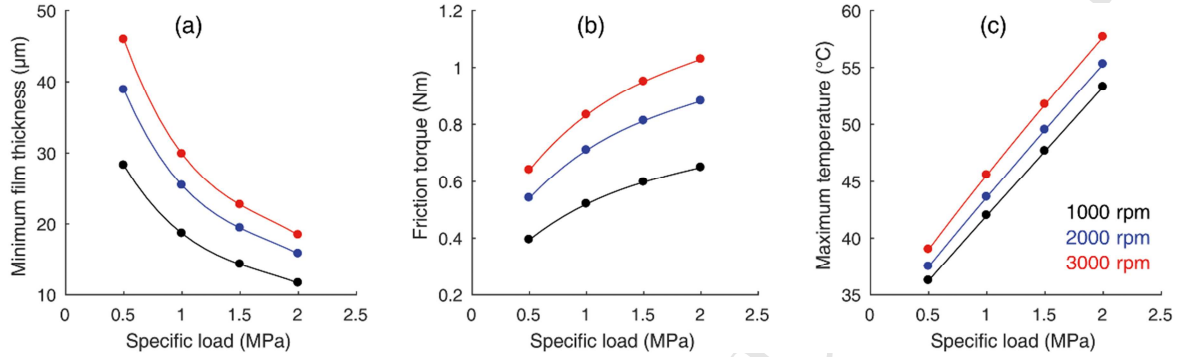

Fig. 10 Performance of the untextured bearing: (a) minimum film thickness, (b) friction torque and (c) maximum temperature.

As expected, the minimum film thickness is proportional to the operating speed and inversely proportional to the applied load. Operating at a specific load of 2.0 MPa and a rotational speed of 1000 rpm, a minimum film of just under 12 µm is predicted. The highest value is predicted for an operation at 0.5 MPa and 3000 rpm (46 µm). Both friction torque and maximum temperature are proportional to the applied load as well as the rotational speed. For the considered bearing, values range from 0.39 to 1.03 Nm and from 36 to 58 °C for T_f and T_{max} respectively.

4.2 Performance of the textured bearing

The relative performance of the textured bearing with respect to the untextured bearing is evaluated for all 108 optimized texture patterns (see Fig. 11).

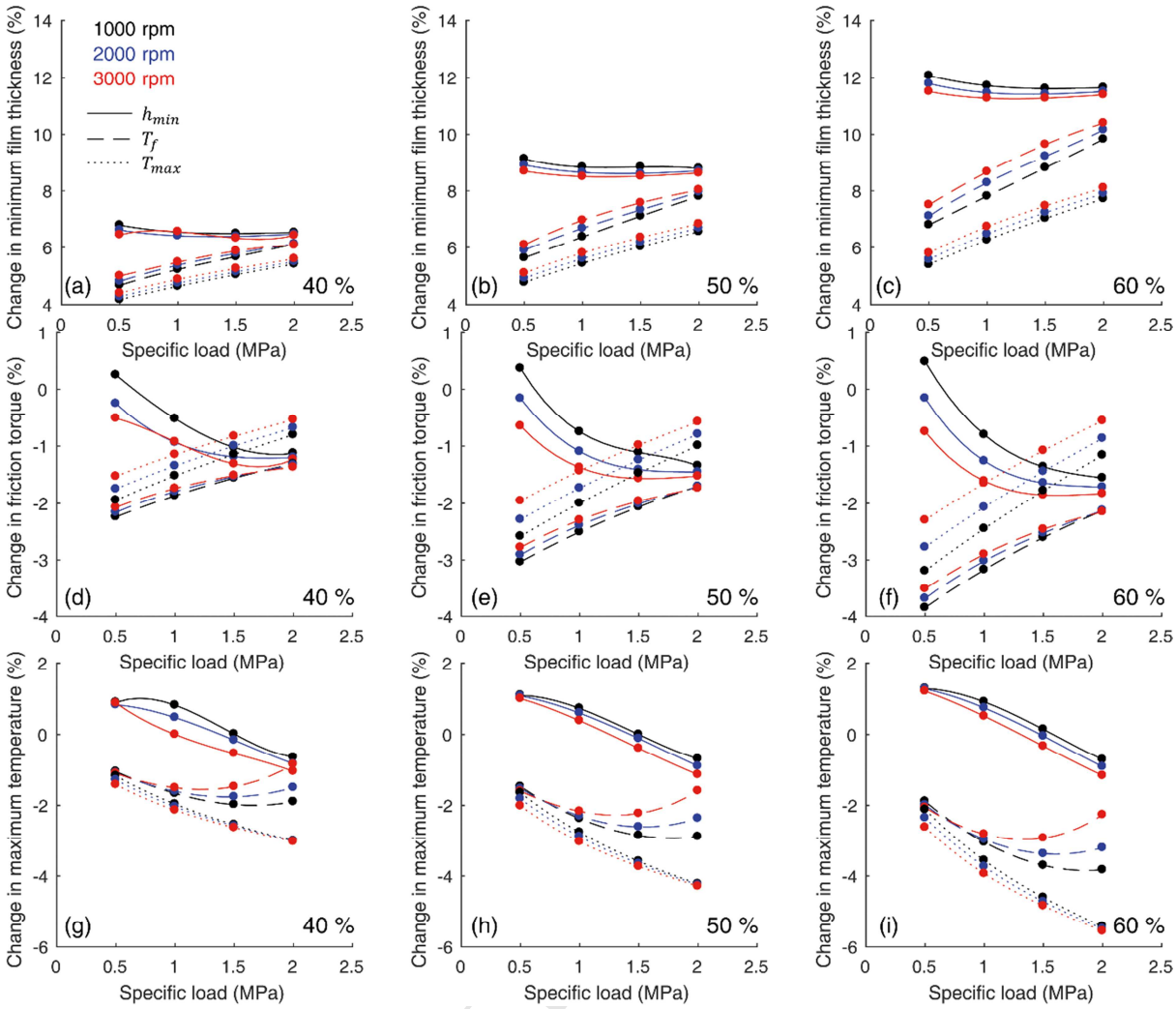

Fig. 11 Performance change caused by texturing: (a)-(c) change in minimum film thickness, (d)-(f) change in friction torque and (g)-(i) change in maximum temperature.

It should be remembered that all considered texture patterns in this graph are optimized for either h_{min}, T_f or T_{max}. Therefore, given results can be interpreted as highest achievable improvements through surface texturing. Note however that a significant degradation in bearing performance may occur if a particular surface design is used under operating conditions it was not designed for. For example, consider the design with 50 % texture density optimized for maximizing h_{min} at 0.5 MPa and 3000 rpm ($h_{texture,opt} = 43$ µm, $\alpha_{opt} = 73$ %, $\beta_{opt} = 70$ %). As shown in Fig. 11, this particular design increases h_{min} by about 9 % while not having a noteworthy influence on friction torque nor temperature. If this pattern was used at 2.0 MPa specific load and 1000 rpm, the minimum film thickness would be decreased drastically by about 14 %. Although the friction torque is not influenced much, the maximum temperature would also be increased by 18 % with respect to the untextured

bearing. This highlights the importance of a thorough texture design for a specific application.

The results also show that the beneficial influence of texturing increases with an increase in texture density for all considered cases. However, this is expected, as it is known for other partially textured contacts that the density cannot be optimized as a higher density will always improve bearing performance [1]. Therefore, the beneficial impact of the considered texture designs could most likely be further enhanced by using higher texture densities. However, this was not done as the density is limited by stress concentration and mixed lubrication considerations.

Interestingly, by far most of the investigated texture patterns improve all three of the considered performance characteristics, independent of the optimization objective, although highest improvements of a particular performance parameter are obviously always achieved by the pattern that was optimized for this parameter. Exceptions to this are the patterns optimized to improve the minimum film thickness, which increase maximum temperature and friction for cases where the bearing operates at low specific loads. Whereas the achievable improvement of the minimum film thickness reaches values of up to 12 %, possible enhancements in terms of friction torque and temperature are rather small, being only about 4 and 6 % respectively, likely not justifying the application of surface textures under hydrodynamic conditions.

It is also noteworthy that the convergence ratio of the pads in equilibrium is no longer determined solely by the pivot position, which is the case for conventional tilting pad thrust bearings. The high influence of the texture extent in circumferential direction on the centre of pressure also entail a dependency of the convergence ratio on the circumferential texture extent, as investigated also by Yagi and Sugimura [19]. Interestingly, the studied texture patterns always decrease the convergence ratio (see Fig. 12).

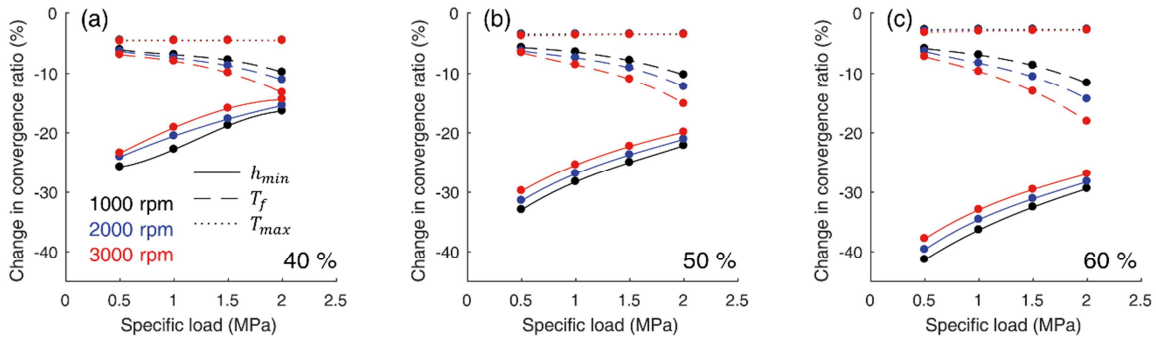

Fig. 12 Change in convergence ratio caused by texturing for different texture densities: (a) 40 %, (b) 50 % and (c) 60 %.

It can be seen that regarding the patterns optimized for T_{max}, the convergence ratio is slightly decreased by approximately 4 % independently from texture density and operating conditions. Slightly higher changes are encountered for the patterns optimized for T_f, being decreased by about 6 % for low load and speed and up to 18 % for high load and speed. The most significant changes in convergence ratio are encountered when the texture pattern is optimized for h_{min}. For a texture density of 40 %, texturing causes the convergence ratio to drop by 14 % to 26 %, depending on the operating conditions. For texture densities of 50 % and 60 % the convergence ratio is decreased by 20 % to 33 % and 27 % to 41 % respectively. In summary, all optimized texture patterns cause the bearing to operate at lower convergence ratios, reaching values of up to 41 %.

5 Conclusions

This paper presents the numerical optimization of surface textures for tilting pad thrust bearings in terms of **texture** depth, circumferential extent and radial extent for various operating conditions and optimization objectives (minimum film thickness, friction torque and maximum temperature). The authors' previously developed fast numerical model based on an adaptive non-uniform finite volume discretization of the Reynolds equation is utilized in combination with an interior-point algorithm to perform a texture design optimization on a normal desktop **computer** within 40 minutes.

The results show that the optimum texture depth depends significantly on the operating conditions and texture density but is mostly independent of the optimization goal. **It is also found that the optimum texture depth should be just slightly smaller than the encountered minimum film thickness of the untextured bearing.** The optimum texture

extent in circumferential direction is largely independent of rotational speed and texture density but does depend on the specific bearing load and the optimization objective. Around 3/4 of the pad should be textured for high minimum film thickness values, just over half of the pad for low friction values and about 2/5 of the pad for low maximum temperatures. The optimum texture extent in radial direction only depends on the applied specific load and the optimization objective. A radial extent of 87 % is recommended for low maximum temperatures and approximately 2/3 of the pad should be textured for both high minimum film thickness and good friction characteristics. Three densities are investigated, where the highest density of 60 % results in **most significant performance improvements**. Whereas minimum film thickness values can be improved by up to 12 %, friction and temperature characteristics can only be improved marginally.

Overall, the results highlight the importance of a proper texture design, which is only possible if the bearing application and predominant operating conditions are known. The presented numerical model allows a fast optimization and initial selection of texture designs. A final texture design may then be chosen based on **additional** CFD simulations or experimental studies. It should be pointed out that the accuracy of the present model may be improved by considering elastic pad deformations and utilizing a more sophisticated thermal model based on the energy and heat transfer equations.

Acknowledgements

The authors acknowledge the financial support of the Engineering and Physical Sciences Research Council (EPSRC) via grant EP/M50662X/1 and John Crane UK Ltd.

References

[1] Gropper D, Wang L, Harvey TJ. Hydrodynamic lubrication of textured surfaces: A review of modeling techniques and key findings. Tribology International. 2016;94:509-29.
[2] Zouzoulas V, Papadopoulos CI. 3-D thermohydrodynamic analysis of textured, grooved, pocketed and hydrophobic pivoted-pad thrust bearings. Tribology International. 2017;110:426-40.
[3] Marian VG, Kilian M, Scholz W. Theoretical and experimental analysis of a partially textured thrust bearing with square dimples. Proceedings of the Institution of Mechanical Engineers, Part J: Journal of Engineering Tribology. 2007;221:771-8.
[4] Henry Y, Bouyer J, Fillon M. An experimental analysis of the hydrodynamic contribution of textured thrust bearings during steady-state operation: A comparison with the untextured parallel surface configuration. Proceedings of the Institution of Mechanical Engineers, Part J: Journal of Engineering Tribology. 2014;229:362-75.
[5] Henry Y, Bouyer J, Fillon M. Experimental analysis of the hydrodynamic effect during start-up of fixed geometry thrust bearings. Tribology International.
[6] Fouflias DG, Charitopoulos AG, Papadopoulos CI, Kaiktsis L, Fillon M. Performance comparison between textured, pocket, and tapered-land sector-pad thrust bearings using computational fluid dynamics

thermohydrodynamic analysis. Proceedings of the Institution of Mechanical Engineers, Part J: Journal of Engineering Tribology. 2014;229:376-97.
[7] Fouflias DG, Charitopoulos AG, Papadopoulos CI, Kaiktsis L. Thermohydrodynamic Analysis and Tribological Optimization of a Curved Pocket Thrust Bearing. Tribology International.
[8] Papadopoulos CI, Efstathiou EE, Nikolakopoulos PG, Kaiktsis L. Geometry Optimization of Textured Three-Dimensional Micro- Thrust Bearings. Journal of Tribology. 2011;133:041702-.
[9] Papadopoulos CI, Kaiktsis L, Fillon M. Computational fluid dynamics thermohydrodynamic analysis of three-dimensional sector-pad thrust bearings with rectangular dimples. Journal of Tribology. 2014;136:011702-1-10.
[10] Gropper D, Harvey TJ, Wang L. A numerical model for design and optimization of surface textures for tilting pad thrust bearings. Tribology International. 2018;119:190-207.
[11] Bartel D. Simulation von Tribosystemen. Wiesbaden: Vieweg+Teubner; 2010.
[12] Ausas RF, Ragot P, Leiva J, Jai M, Bayada G, Buscaglia GC. The Impact of the Cavitation Model in the Analysis of Microtextured Lubricated Journal Bearings. Journal of Tribology. 2007;129:868-75.
[13] Arghir M, Alsayed A, Nicolas D. The finite volume solution of the Reynolds equation of lubrication with film discontinuities. International Journal of Mechanical Sciences. 2002;44:2119-32.
[14] Dobrica MB, Fillon M. About the validity of Reynolds equation and inertia effects in textured sliders of infinite width. Proceedings of the Institution of Mechanical Engineers, Part J: Journal of Engineering Tribology. 2009;223:69-78.
[15] Stachowiak GW, Batchelor AW. Engineering Tribology. 4th ed. Amsterdam; London: Elsevier/Butterworth-Heinemann; 2014.
[16] Frene J, Nicolas D, Degueurce B, Berthe D, Godet M. Hydrodynamic Lubrication: Bearings and Thrust Bearings: Elsevier Science; 1997.
[17] Glavatskih SB, Fillon M, Larsson R. The Significance of Oil Thermal Properties on the Performance of a Tilting-Pad Thrust Bearing. Journal of Tribology. 2001;124:377-85.
[18] Mathworks. Dokumentation: fmincon, https://uk.mathworks.com/help/optim/ug/fmincon.html. accessed 08.12.2017.
[19] Yagi K, Sugimura J. Performance of Balancing Wedge Action in Textured Hydrodynamic Pad Bearings. Journal of Tribology. 2016;139:011704-.

List of Figures with captions, resolution (w x h), preferred size (w x h) and dpi

Fig. 1 Pad details with coordinate system, (b) tilting pad thrust bearing geometry and (c) exemplary texture pattern with $\alpha = 70\ \%$, $\beta = 70\ \%$, $h_{texture} = 10\ \mu m$ and $\rho_{texture} = 40\ \%$.

Resolution: 2165 x 1772 Preferred size: 11 x 9 cm DPI: 500

Fig. 2 Computational mesh with 4 x 4 control volumes inside individual textures, 2 x 2 control volumes in-between adjacent textures, 8 control volumes for the untextured pad area in circumferential direction and 4 control volumes each for the untextured pad areas in radial direction.

Resolution: 1772 x 1378 Preferred size: 9 x 7 cm DPI: 500

Fig. 3 Simplified flow chart for the numerical texture design optimization.

Resolution: 1181 x 2165 Preferred size: 6 x 11 cm DPI: 500

Fig. 4 Results of the mesh study for texture densities of 40%, 50% and 60%.

Resolution: 1772 x 1772 Preferred size: 9 x 9 cm DPI: 500

Fig. 5 Validation of the optimization algorithm for the three optimization objectives: (a) minimum film thickness, (b) friction torque and (c) maximum temperature.

Resolution: 1772 x 2953 Preferred size: 9 x 15 cm DPI: 500

Fig. 6 Optimum texture depth for different operating conditions and optimization objectives for a texture density of (a) 40 %, (b) 50 % and (c) 60 %.

Resolution: 3740 x 2165 Preferred size: 19 x 11 cm DPI: 500

Fig. 7 Relative optimum texture depth for different operating conditions and optimization objectives for a texture density of (a) 40 %, (b) 50 % and (c) 60 %.

Resolution: 3740 x 2165 Preferred size: 19 x 11 cm DPI: 500

Fig. 8 Optimum circumferential texture extent for different operating conditions and optimization objectives for a texture density of (a) 40 %, (b) 50 % and (c) 60 %.

Resolution: 3740 x 2165 Preferred size: 19 x 11 cm DPI: 500

Fig. 9 Optimum radial texture extent for different operating conditions and optimization objectives for a texture density of (a) 40 %, (b) 50 % and (c) 60 %.

Resolution: 3740 x 2165 Preferred size: 19 x 11 cm DPI: 500

Fig. 10 Performance of the untextured bearing: (a) minimum film thickness, (b) friction torque and (c) maximum temperature.

Resolution: 3740 x 1082 Preferred size: 19 x 5.5 cm DPI: 500

Fig. 11 Performance change caused by texturing: (a) - (c) change in minimum film thickness, (d) - (f) change in friction torque and (g) - (i) change in maximum temperature.

Resolution: 3740 x 3248 Preferred size: 19 x 16.5 cm DPI: 500

Fig. 12 Change in convergence ratio caused by texturing for different texture densities: (a) 40 %, (b) 50 % and (c) 60 %.

Resolution: 3740 x 1082 Preferred size: 19 x 5.5 cm DPI: 500

Research highlights of the paper with title:

Numerical analysis and optimization of surface textures for a tilting pad thrust bearing

- Texture patterns are optimized in terms of texture depth, circumferential extent and radial extent.
- Three optimization objectives are considered: minimum film thickness, friction torque and maximum temperature.
- For most cases, optimum texture parameters depend on the operating conditions, optimization objective and texture density.
- The minimum film thickness can be improved by up to 12 %.
- Only marginal improvements are possible with regards to friction torque and maximum temperature.